Tectonophysics 722 (2018) 235–248

Contents lists available at ScienceDirect

Tectonophysics

journal homepage: www.elsevier.com/locate/tecto

Regional variation of coda *Q* in Kopili fault zone of northeast India and its implications

Nilutpal Bora[a], Rajib Biswas[a,*], Anna A. Dobrynina[b]

[a] Geophysical Lab, Department of Physics, Tezpur University, Tezpur 784028, Assam, India
[b] Institute of the Earth's crust SB RAS, 128 Lermontov Street, 664033 Irkutsk, Russia

ARTICLE INFO

Keywords:
Coda-wave
Wave propagation
Frequency dependency
Seismic attenuation
Crustal properties

ABSTRACT

Kopili fault has been experiencing higher seismic and tectonic activity during the recent years. These kind of active tectonics can be inspected by examining coda-wave attenuation and its dependence with frequency. Exploiting single back-scattering model, we have endeavored to measure coda *Q* and its associated parameters such as frequency dependent factor (*n*) and attenuation coefficient (γ) covering seven lapse-time windows spanning from *30* to *90* s and central frequencies *1.5*, *3.5*, *6*, *9* and *12* Hz. The average estimated values of Q_C increases with frequency and lapse time window from *114* at frequency *1.5* Hz to *1563* at frequency *12* Hz for *30* s window length, and from *305* at frequency *1.5* Hz to *2135* at frequency *12* Hz for *90* s window length. The values of Q_0 and n are also estimated for the entire Kopili fault zone. For this study region, the Q_0 values vary from *62* to *348* and *n* varies from *0.57* to *1.51* within the frequency range *1.5* to *12* Hz. Furthermore, depth variation of attenuation of this region reveals that there is velocity anomaly at depth *210–220 km* as there arises sharp changes in γ and *n* which are supported by available data, reported by other researcher for this region. Finally, we have tried to separate the intrinsic and scattering attenuation for this area. It is observed that the entire region is dominated by mainly scattering attenuation, but we can see an increase in intrinsic attenuation with depths in two stations namely TZR and BKD. Furthermore, the obtained results are comparable with the available global data.

1. Introduction

The energy of seismic wave at various distances from earthquake source is severely affected by geological medium. Attenuation is one of the vital parameters that characterizes the medium through which seismic wave propagates. It is defined as the dissipation of seismic energy while traversing from the earthquake source to the receiver. This dissipation continues until the seismic wave disappears due to loss of energy (or loss of amplitude). The energy of seismic waves decays due to the geometrical spreading, intrinsic and scattering attenuation (Sedaghati and Pezeshk, 2016; Padhy et al., 2011). The decrease in amplitude of the seismic waves, caused by the geometrical spreading in a homogeneous and isotropic medium, is inversely proportional to the distance travelled. While intrinsic attenuation converts the seismic energy into heat due to inelastic absorption, scattering or elastic attenuation redistributes the energy at random heterogeneities present in the earth's crust. It should be pointed out that the total energy in the wavefield remains constant in case of scattering attenuation, whereas the intrinsic attenuation causes disappearance of the wave due to loss of energy. Therefore, attenuation of seismic waves in the earth's crust is a key phenomenon for understanding the diversity in the earth's physical states and seismic potential of the region (Singh and Hermann, 1983; Parvez et al., 2008). The attenuation property of the medium is usually measured by a dimensionless quantity, called the quality factor *Q*, which is defined as the ratio of wave energy to the energy lost per harmonic oscillations (Knopoff and Hudson, 1964; Aki and Chouet, 1975) while propagating through the intermediate medium. The attenuation of medium is inversely proportional to the quality factor (*Q*) which means that, seismic waves are highly attenuated for regions having lower *Q* values.

Attenuation parameter (*Q*) can be characterized by *P*-wave quality factor (Q_P), *S*-wave quality factor (Q_S), and coda-wave quality factor (Q_C). Several researchers have carried out extensive research by using various methods in order to investigate the mechanism of coda wave attenuation in the earth's lithosphere. Aki (1969) and later, Aki and Chouet (1975) first estimated Q_C from the tail portion of the seismogram. They (Aki, 1969; Aki and Chouet, 1975; Rautian and Khalturin, 1978) estimated Q_C based on the fact that coda wave was caused by

* Corresponding author.
E-mail address: rajib@tezu.ernet.in (R. Biswas).

https://doi.org/10.1016/j.tecto.2017.11.008
Received 23 May 2017; Received in revised form 2 November 2017; Accepted 4 November 2017
Available online 09 November 2017
0040-1951/

scattering of seismic waves from numerous randomly distributed heterogeneities in the Earth's crust and the upper mantle. On the other hand, Sato (1987), Guo et al. (2009); Jin and Aki (1988) and Novelo-Casanova et al. (2006) suggested the changes in Q_C as a precursor to major earthquakes.

Numerous studies have been carried out in order to estimate Q_C, the quality factor of the coda wave, for different parts of the world (Aki and Chouet, 1975; Sato, 1977; Bianco et al., 2002; Kumar et al., 2016a; Gupta et al., 1995; Kumar et al., 2005; Hazarika et al., 2009; Sharma et al., 2009; Mukhopadhyay and Sharma, 2010; Padhy and Subhadra, 2010; Tripathi et al., 2012; Singh et al., 2012; Hazarika et al., 2013). Apart from this, Aki (1969), Aki and Chouet (1975) and Sato (1977) opined that analysis of coda wave of local earthquakes enables us to study the seismic wave attenuation in the crust and lithosphere. However, not much study on the attenuation property of the crust and lithosphere is made in the North East India (NER) region with special reference to Kopili region. Till now, only a handful of literatures are available (Hazarika et al., 2009; Padhy and Subhadra, 2010; Biswas et al., 2013a,b). The Kopili Fault Zone in Northeast India, is an intraplate earthquake source zone and is characterized as a potential zone for a large impending earthquake. Till now, this fault generated two large earthquake [as shown in Fig. 1 (b)] and several intermediate earthquake. This makes it a probable region for earthquake damages, and it would be useful to study attenuation characteristics of this region in order to make it available for other scientists who would be interested in hazard zonation/microzonation of this area. The regional values of coda Q and its spatial variation is directly related to tectonics and seismicity, playing a vital role in seismic risk analysis and engineering seismology (Singh and Hermann, 1983; Jin and Aki, 1988). To the best of our knowledge, such type of study has not been conducted in this seismically active area. Only, Bora and Biswas (2017) quantified regional body wave attenuation for this Kopili region using direct P and S-wave. As a part of quest to understand the mechanism of crust and lithosphere, an attempt has been made in order to obtain information on the seismic wave attenuation parameters in the lithosphere and upper mantle of this Kopili Fault zone from S-wave coda of local earthquakes using the single backscattering model. Further, depth variation of coda Q is also examined. In addition, we have also looked into the lapse time dependence of coda Q. While addressing these issues, we have comprehensively analyzed the correlation of coda Q with temperature, accompanied by global data to apprehend the inherent mechanism.

2. Seismotectonics

North East India (NE, India) is one of the seismically active regions in the world where *16* large (M ≥ 7.0) and two great earthquakes [i.e.1897 (MS *8.7*) (Oldham, 1899) and 1950 (MS 8.6) (Poddar, 1950)] occurred during the last century. This region comprises of distinct geological units, like the Himalayan frontal arc to the north, the highly folded Indo-Burma mountain ranges or Burmese arc to the east, the Brahmaputra River alluvium in the Assam valley and the Shillong–-Mikir plateau in between these two arcs, and thick sediments of the Bengal basin to the south. Among those major earthquakes occurring in NE India and its neighborhood, Kopili fault zone had already witnessed two major earthquakes [as shown in Fig. 1(b)] of magnitude > 7 (MS). It is bounded by latitude 25.50° to 27° N and longitude 92° to 93° E. The first major earthquake of magnitude 7.8(MS) occurred on 10th of January 1869 (GSI) having a depth of *60 km*, this event incurred severe damages encompassing Dhubri to east of Imphal. Even, Nagaon and Silchar region also suffered huge losses as per reports. However, the epicenter is located at *25.250 N*: *93.250E* (unpublished report). The second event occurred in 1943 with a magnitude of ~7.3 along the Kopili fault. As per Kumar et al. (2016b) and Bora and Biswas (2017); during Mesozoic to tertiary era, this study area evolved. As documented, there is no surficial signature of Kopili fault other than a topographic depression. Another distinct geological feature is that, the Mikir Hills is separated from Shillong Plateau by Kopili fault which trend in the NW-SE direction. With an approximate length of *300 km* and width of *50 km*; the Kopili fault extends from western part of Manipur to tri-junction of Bhutan, Arunachal Pradesh and Assam. Very recently Singh et al. (2017) cited about the role of Kopili fault in the recent Imphal earthquake. As reported by Kayal et al. (2006), high level of seismic activity exists within the Kopili fault and it was found that events pertaining to Kopili fault zone were characterized by a depth ~*50 km* below the Kopili fault (Kayal et al., 2006, 2010). Bhattacharya et al. (2008) estimated three-dimensional (3D) P-wave velocity (V_P) structure of the north-east India and estimated that the Kopili fault system extends from *20* to *30 km* depth and there is a high V_P structure below Mikir Hills at a depth of *40 km*. As per Kundu and Gahalaut (2013), the Kopili fault located to the east of the SP is also undergoing active deformation with a slip of 2.9 ± 1.5 *mm/year*. The Kopili fault was also found to have a normal and strike slip faulting with a dip in the north-eastern direction. The recent seismicity discovered along the fault has led to speculations that the Kopili fault is one of the most seismically active faults of the region and a major earthquake could be expected in the future (Kayal et al., 2006, 2010).

3. Dataset

The present dataset consists of *300* digital seismograms of small to moderate earthquakes with magnitude M_L = *2.1–3.9*, recorded by six stations (Table 1) within an epicentral distance ~*180 km*. This network of stations is operated by National Geophysical Research Institute (NGRI), Hyderabad. All the six stations are equipped with three component Broadband Seismographs with GPS synchronized timings. The data were sampled with a digitizing frequency of *100* samples per second. The corresponding epicentral plot and ray path distribution are provided in Fig. 1(b) and (c), respectively. As seen, the events are scattered with decent azimuthal coverage around the receiver sites under consideration. As reported by Negi et al. (2014), such sort of spreading helps in elimination of impact of source radiation pattern to best possible level. Besides, the seismograms of all well-located events were carefully inspected to ease any overlapping, or early cutoff. Further, emphasis is given to those events having signal to noise ratio greater than ~*2*. Velocity model of Bhattacharya et al. (2008), compatible for Kopili region has been employed with a view to determining the hypocentral parameters. The depths of the events vary from *8.3* to *42 km*. The root mean square value for hypocentral parameter estimates is below *0.2 s*.

4. Methodology

We have adopted the single backscattering model of Aki and Chouet (1975) to measure seismic wave attenuation from the coda wave. It is assumed that the coda waves arises from superposition of scattered direct S-waves reflected by the heterogeneities randomly distributed in the crust and the upper mantle (Aki, 1969; Rautian and Khalturin, 1978). One of the main assumption of this model is that ~*1* Hz, coda waves are the backscattered surface waves and at *10* Hz and onwards, they becomes backscattered body waves produced within medium due to randomly distributed heterogeneities. In this model, the amplitude of coda wave (A_C) at a central frequency f for a desired frequency band and a specific lapse time t measured from the earthquake origin time t_0 can be expressed as,

$$A_C(f,t) = S(f)G(f)I(f)\left[t^{-\alpha}e^{\left(-\frac{\pi f t}{Q_C(f)}\right)}\right] \quad (1)$$

where, $S(f)$, $G(f)$, $I(f)$ represent the source response, site amplification and instrument response. The geometrical spreading parameter α is considered to be unity in this study as suggested by Havskov et al.

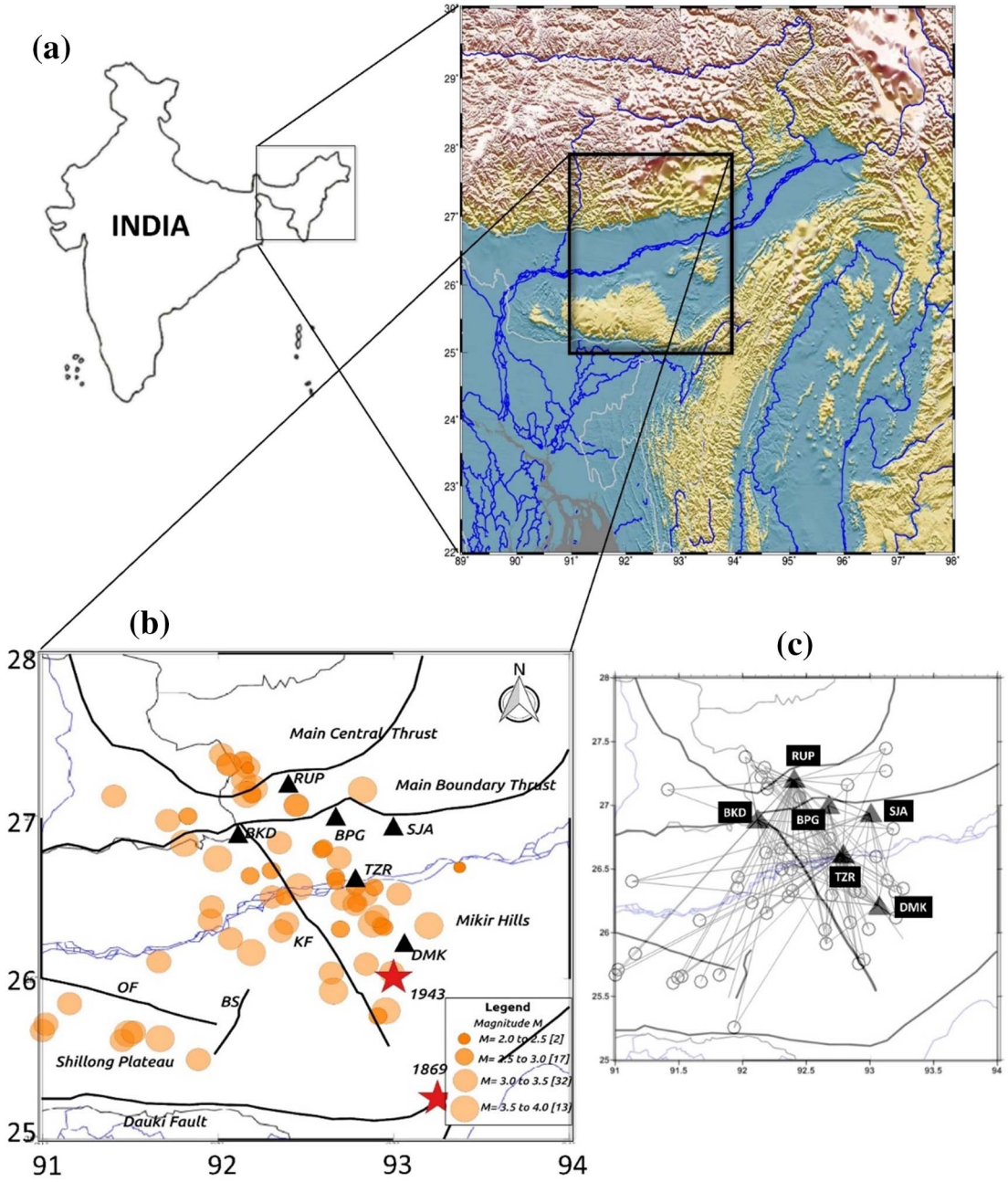

Fig. 1. (a) Simplified map of Northeast India. (b) Map showing major tectonic features of Kopili Fault region [after Biswas et al., 2013 a,b.]. These are designated as: Main Boundary Thrust (MBT), Main Central Thrust (MCT), Dauki fault, Kopili fault (KF), Oldham fault (OF), Borapani Shear Zone (BS). The filled circles represent the epicenters used for our study and triangles represents the stations temporarily deployed in Kopili region. The star symbols represent the Great and major earthquakes originating in and around Shillong Plateau. (c) Maps showing the distribution of ray paths connecting the events (circles) and stations (triangles) used in this study.

(1989), since coda waves are considered as backscattered body waves (Aki, 1980, 1981). The term Q_C represents coda wave quality factor which characterizes average attenuation of the medium for a pre-defined region.

The terms $S(f)$, $G(f)$, $I(f)$ are time independent, so if we take natural logarithm of them then the natural logarithm of the multiplication of them is also time independent. It should be pointed out that the coda wave amplitudes are independent of source radiation pattern (Aki, 1969). Again, as we have used only small to moderate earthquakes (*2.1–3.9* ML), so they have small focal volume (small magnitude) which too facilitate ignoring the effect of radiation pattern. As Hanks and McGuire (1981) already reported that the link between high-frequency amplitude and radiation pattern is negligible for small magnitude earthquakes. By taking the natural logarithm of Eq. (1) and rearranging the terms, the equation can be rewritten as,

$$ln[A_C(f,t) \times t] = c - bt \quad (2)$$

This is a simple linear equation where $b = \frac{\pi f}{Q_C(f)}$ and $c = \ln[S(f)G(f)I(f)]$. Thus Q_C can be determined from the slope of the least square fit corresponding to the plot of $\ln[A_C(f,t) \times t]$ versus t.

As described by Stewart (1984), Scherbaum and Kisslinger (1985) and Gupta et al. (1998) the estimated Q_C represents the average decay of amplitude of the back-scattered wave for an ellipsoidal volume where the earthquake source and receiver are located at its focus. Therefore, the surface area of this ellipsoidal volume inside which the coda waves are distributed can be represented using the following equation:

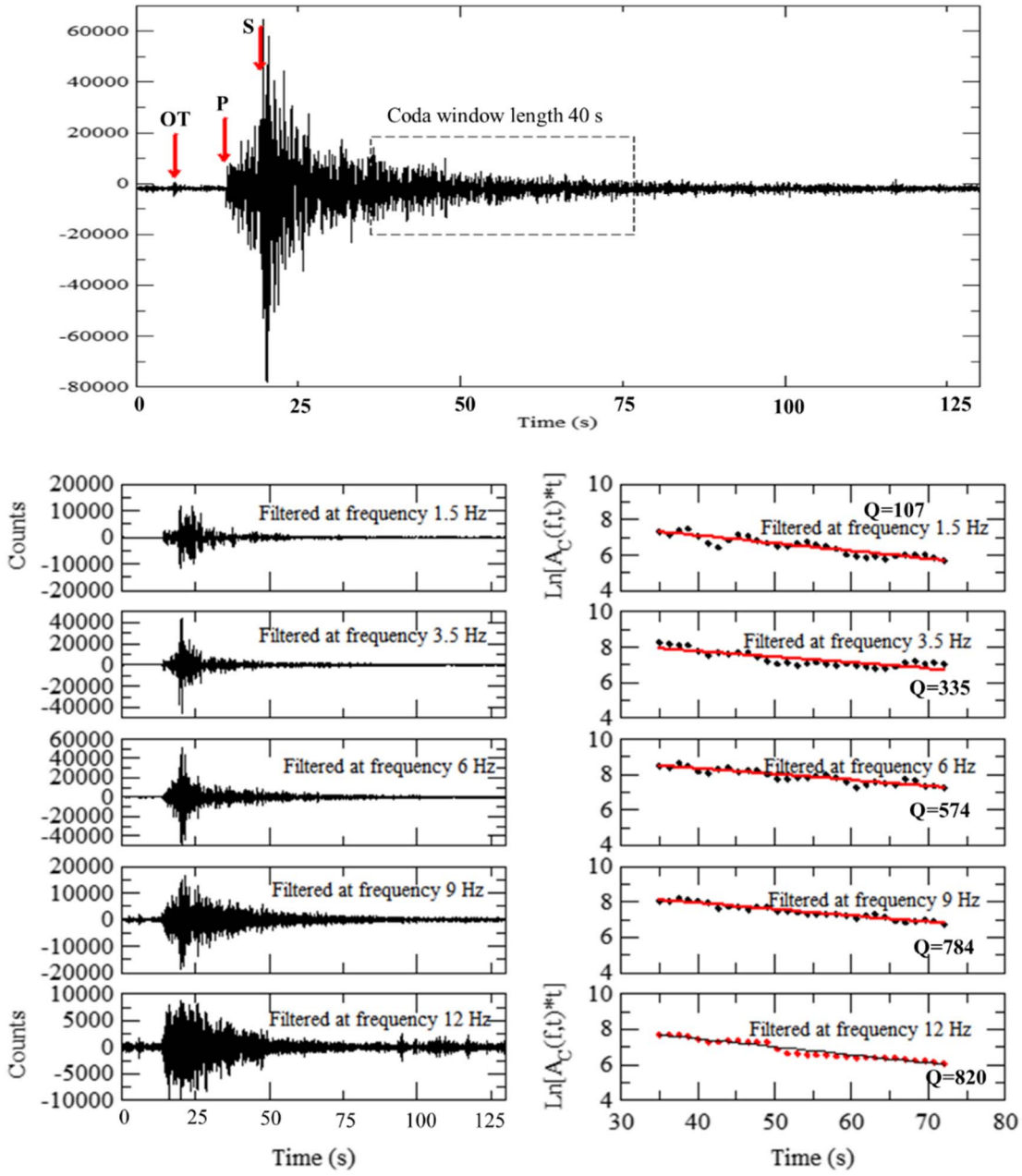

Fig. 2. An example of coda processing for Q_C estimation for the 01 March 2003 earthquake (25.65° N; 91.49° E; M 3.74; and 42 km depth) recorded at station RUP. Top: original (non-filtered) seismogram (vertical component). Arrow shows the origin time, *P*-wave arrival, *S*-wave arrival of the event and bracket shows the analyzed part of the coda. Bottom left: filtered seismograms (frequency bands *1–2*; *2–5*; *4–8*; *6–12*; *9–15* Hz, respectively). Right: amplitudes of filtered coda-wave versus time and corresponding regression lines obtained by least square method for lapse time window length of *40* s. For each frequency range, Q_C-value and central frequency are shown.

$$\frac{x^2}{a^2} + \frac{y^2}{b^2} = 1 \tag{3}$$

where, $a = vt/2$ and $b = \sqrt{a^2 - \frac{\Delta^2}{4}}$. Here, v, Δ and t represents the *S*-wave velocity, average hypocentral distance and average length of the lapse time. In general, the average lapse time is taken as $t = t_0 + \frac{W}{2}$ (where t_0 stands for starting time of coda window and w is the coda window length). It is seen that if the value of Δ equals to zero than the above equation represent a circular area of radius $vt/2$. The lower border of this ellipsoid or the maximum depth of this assumed ellipsoid represent the penetration depth of the estimated coda wave quality factor (Havskov et al., 1989) and can be calculated by $h = h_{avg} + b$ in which h_{avg} is the average earthquake depth.

5. Data analysis

As reported by Sato and Fehler (1998) and Sedaghati and Pezeshk (2016), there is slight difference between vertical and horizontal components of the *S*-coda envelopes of small earthquake. For simplicity, we have only used the vertical components for our study. Each seismogram was bandpass-filtered at five frequency bands (*1–2*; *2–5*; *4–8*; *6–12*; *9–15* Hz) with central frequencies at *1.5*, *3.5*, *6*, *9* and *12* Hz (Table 2), by using a fourth-order Butterworth filter respectively. Then, the coda amplitudes $A_C(f,t)$ were calculated by smoothing the coda windows of all filtered seismograms using a root-mean-square (RMS) technique (Zelt et al., 1999; Sharma et al., 2009; Kumar et al., 2005). Frankel (2015) demonstrated that usage of RMS values gives more stable results as compared to direct Fourier transform. The RMS value of the amplitudes is evaluated for a moving window with a length of

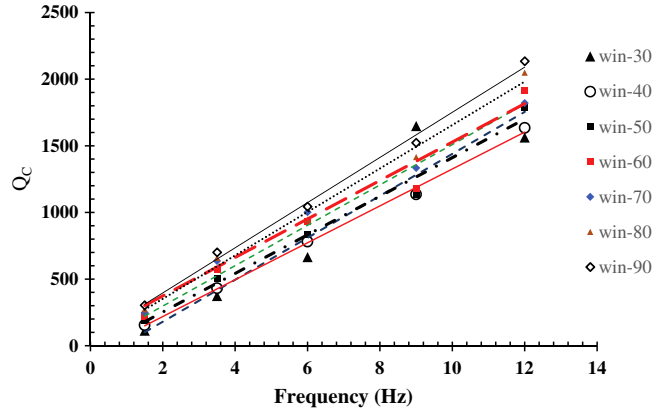

Fig. 3. Plot of the mean Q_C values of each lapse time window versus frequency.

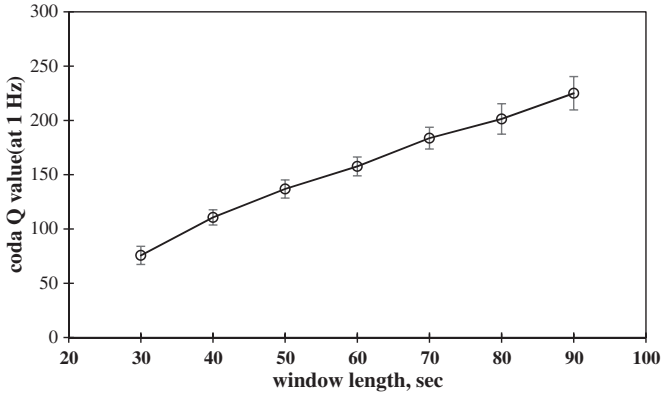

Fig. 4. Plot of quality factor Q_C at the frequency of *1* Hz versus lapse time window.

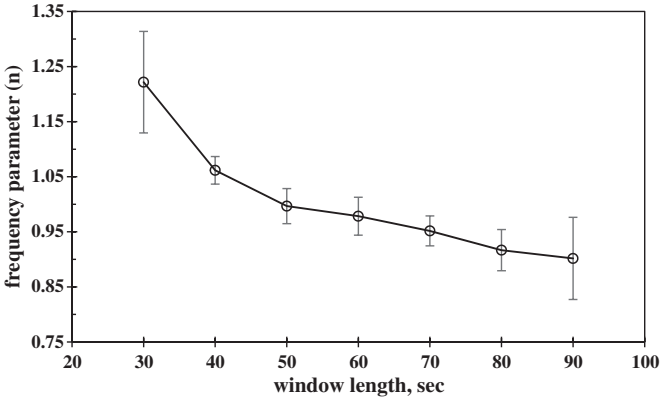

Fig. 5. Plot of frequency parameter (n) versus lapse time window.

2.56 s centered at lapse time t to generate a smoother coda envelope. Then, the moving window slides along the coda window with steps of *1.28* s. We do not use all RMS values obtained from the moving window and discard centers in which the RMS value to noise ratio is < 2. The lapse time windows of the coda wave used in this study are started from $2t_S$ (where t_S is the *S*-wave travel time) in order to avoid contamination of direct *S*-wave (See Fig. 2) and scattered waves (Rautian and Khalturin, 1978). As it was reported that if the starting of the lapse time window is taken in between t_S and $2t_S$, then there is a possibility of near-site reverberations to become dominant (Spudich and Bostwick, 1987). It is observed (Pulli, 1984; Del Pezzo et al., 1990; Woodgold, 1994) that the value of Q_C increased with increasing lapse time. Havskov and Ottemoller (2005) advised a minimum value of *20* s for the coda window length in order to obtain stable results. In this study, we have used seven lapse time window length which vary from *30* to *90* with increments of *10* s. Although there is generally no limit on the maximum lengths of the coda window, the values of SNR > 2 condition for most of the seismograms in this study cannot be satisfied for coda window lengths > 90 s. Thus, the upper limit has been fixed to *90* s.

After taking the smoothed values of coda amplitude for the centers of each sliding windows, Q_C can be obtained from the slope of the straight line of Eq. (2) at each central frequency. Towards estimation of Q_C, we have obtained few negative values which are rejected (Woodgold, 1994).

6. Results and discussion

For each station, using vertical component of the seismogram, we have estimated the values of Q_C as a function of frequency. The average estimated values of Q_C have been mentioned in the Table 3 for different window lengths from *30* to *90* s with an increment of *10* s. For window length of *30* s, the average value of Q_C increases from *114* at frequency *1.5* Hz to *1563* at frequency *12* Hz. Similarly, an increasing trend in Q_C is observed for all the lapse time window up to *90* s.

In order to observe this frequency dependency of Q_C, by using the estimated values of Q_C for all station and plotting them against their central frequency, we made the empirical power law for Q_C in the form of $Q_C(f) = Q_0 f^n$ where n is the frequency dependent coefficient and Q_0 is the value of Q_C at *1* Hz. The estimated values of Q_0 and n for all window length are enlisted in the Table 4. It is observed that the values of Q_C increase with increase in frequency. The errors in Q_C and n are also listed in Table 4. It is clear that the values of Q_0 increases with increased frequency. The obtained power law form for our study region are given in the Table 3. In the discussion to follow, we have taken into account all parameters influencing coda quality factor.

6.1. Dependency with frequency:

In this study area, we have noticed a strong frequency dependence of estimated Q_C (Fig. 3, Table 3) as our estimated values of Q_C show a clear increase with frequency for all the six stations. It is implicit that the frequency dependent parameter (n) is not constant for Kopili region (Table 4). Other studies found that the n values become larger in tectonically active regions like NE-India (Hazarika et al., 2009; Padhy and Subhadra, 2010). In Kopili region, the frequency dependent relation comes out to be $(63 \pm 6)f^{(1.33 \pm 0.11)}$ for *30* s window and $(213 \pm 5)f^{(0.91 \pm 0.03)}$ for *90* s window. As such, it can be summarized that the obtained values of frequency dependent parameter in Kopili region are ~ 1, indicating that the region is highly heterogeneous and tectonically very active.

6.2. Dependency with Lapse time window

In our study region, it has been observed that the estimated values of Q_C increases with lapse time and are irregular. The average value of Q_C for the study region varies from *114* at *1.5* Hz to *1563* at *12* Hz for a lapse time of $2t_S$ and corresponding coda window length of *30* s. When the window length is increased, then Q_C also rises with respect to frequency. For instance, at *1.5* Hz and *12* Hz, the obtained values are *304* and *2135* corresponding to a window length of *90* s. This observation of frequency dependence of Q_C is due to the degree of heterogeneity of the medium and the level of tectonic activity in the area (Aki, 1980). The low Q_C values or high attenuation at lower frequencies may indicate a high degree of heterogeneity and a decrease in rock strength in the shallow regions.

This increase in Q_C with increase in window length (Table 3) may be linked to the increase in Q_C with depth, as it was already reported that the larger is the window length, the larger is the sampled area of the earth's crust and mantle. Fig. 4 shows the variation of Q_0 with lapse time window length.

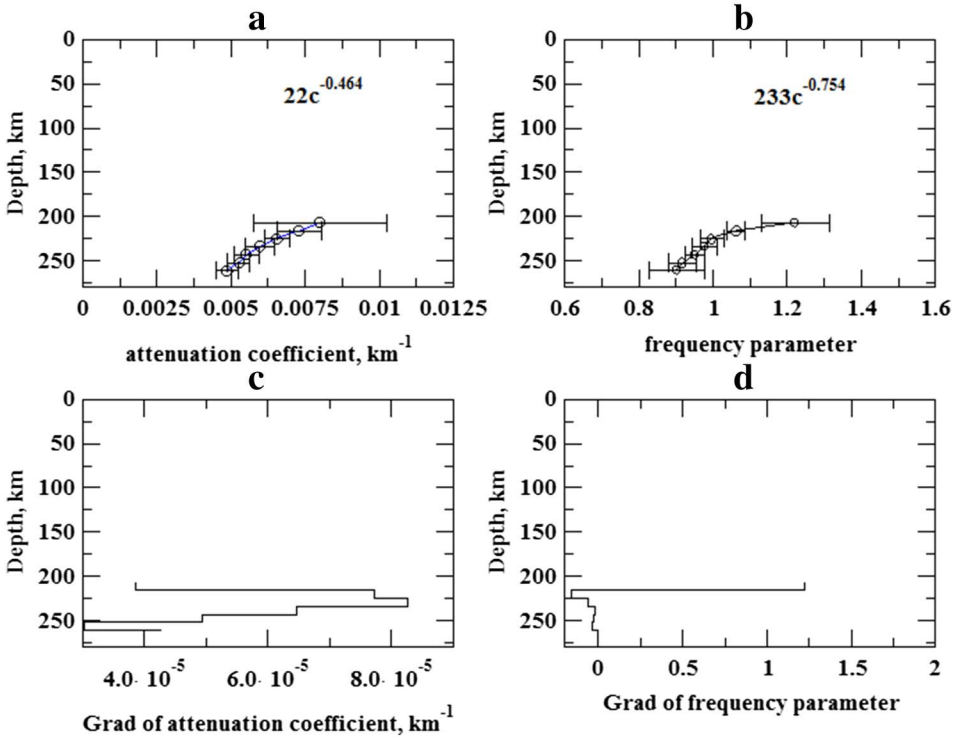

Fig. 6. Vertical variations of the attenuation parameters: attenuation coefficient (a) and frequency parameter (b) versus depth of the lower boundary of the ellipsoid. Error on each value are shown. Bottom: gradients of the attenuation coefficient (c) and frequency parameter (d) versus depth.

On the contrary, value of n is not constant for this region (Fig. 5) and is inversely proportional to the length of lapse time window. The main fact of this could be due to scattered seismic waves that reach the station from greater depths.

6.3. Variation with depth

A rough estimate of maximum depth through lapse time and average epicentral distance is achieved using the Eq. (3). Here, we have taken $v = 3.5$ *km/s* (Gupta et al., 1984). The value of w is taken from *30* to *90* s. Table 5 lists the values of the axis for all the stations for varying window length. It is observed that the values of the axis are almost equal, and thus we can considered the ellipsoidal volume practically spherical. From the Table 5 we can see that the depth of coda formation varies from *207 km* down to *261 km*. As it was already mentioned that attenuation increases with increasing lapse time window, as lithosphere becomes more homogeneous with depth (Pulli, 1984; Irandoust et al., 2016). Higher values of penetration depth, as obtained by us, imply that the estimated values of Q_C for all the stations are characteristic of whole crust and earth's upper mantle beneath the Kopili fault zone. For maximum source to station distance, our estimated Q_C values represent the average attenuation property of the spherical volume with areas up to *181,468* km^2. Steck et al. (1989) reported that the variation of Q_C may be due to path effect, as the obtained values of coda volumes are distinct and sample different geological structure.

From Fig. 6(a) and (b) it is observed that the attenuation coefficient γ and the frequency parameter n behaved differently with varying penetration depth. From their respective power law as mentioned in Fig. 6(a) and (b), it can be opined that attenuation decreases with increase in penetration depth in the upper layer of the earth's mantle. Similarly the frequency parameter decreases with increasing depth. This could be also attributed to a depth-wise increase in degree of homogeneity, which in turn would lead to an increase in the density of large scatterers (Dasović et al., 2013).

In Fig. 6(c) and (d) we noticed that there is a sharp variation of the values of gradient of γ and n at depth *210–220 km*. This variation may be attributed to velocity discontinuity. Similar behavior of γ and n were reported for other region due to change in velocity (Dobrynina et al., 2016 for Baikal rift zone; Dobrynina, 2013 for Basin and range Province). Another plausible reason for this variation may be ascribed to either prevalence of strong heterogeneity in the lithospheric mantle or possibly significant variations of rock composition and temperature in the uppermost mantle. This conjecture gets further validation from the report of Wei et al. (2016) where they hinted at significant variation of FVD (Fast velocity direction) in the Indian lithosphere in the depth range of *60–200 km*, implicating anisotropy. Ramesh et al. (2005) gave a hypothesis in order to explain presence of seismic discontinuities in the depth range over *250 km* invokes interplay of an implicit low velocity zone. They (Ramesh et al., 2005) reported that another possibility of this discontinuity may involves the anomalous nature of melt migration and segregation at high pressure and temperatures corresponding to depth as large as *180–300* km.

6.4. Lateral and spatial variation of coda Q

In this study, coda Q variation and its frequency dependence are determined in the study region using events recorded at six stations along the Kopili fault. In order to carry out this we have chosen identical epicentral range in each data set. This is essential because longer rays penetrate to greater depths, where attenuation might be different, and two stations with similar attenuation properties around them could show different Q_0 if one receives rays from farther distances. Table 1 shows the average epicentral distance of each station. In order to have similar epicentral distance we have selected only those so that the average epicentral distance remain in the range of *80* to *90 km*.

We constructed a map of coda Q and n (frequency parameter) corresponding the six stations as marked in Figs. 7(a) and 8(a) along the Kopili fault zone using spatial smoothing of *1* min × *1* min in longitude and latitude to examine details of the spatial variation in the study area. In Japan, such studies have been done nicely in recent works of coda Q (e.g. Jin and Aki, 2005; Carcolé and Sato, 2010; Hiramatsu et al., 2013; Dojo and Hiramatsu, 2017).

Fig. 7 and 8 display the contour plot of average values of Q_0 and n for all the six stations with diverse coda window lengths. For *30* s

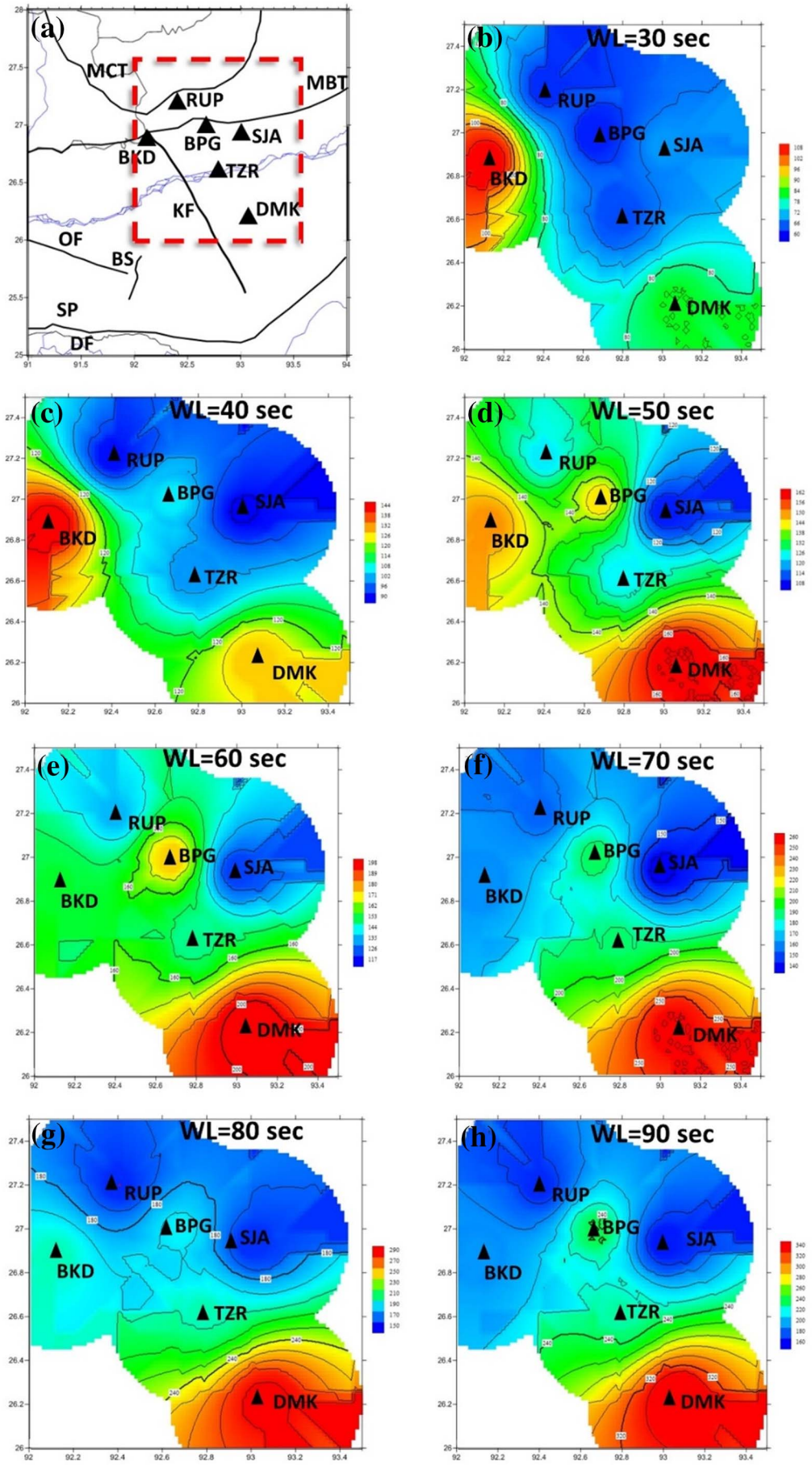

Fig. 7. (a) The study region and the dotted box represents the area selected for the contour plot. (b) to (h) Examples of the spatial distribution of coda Q_o. Triangles are stations used to draw maps. The scale indicates the maximum and minimum values of Q_o obtained for each coda window length.

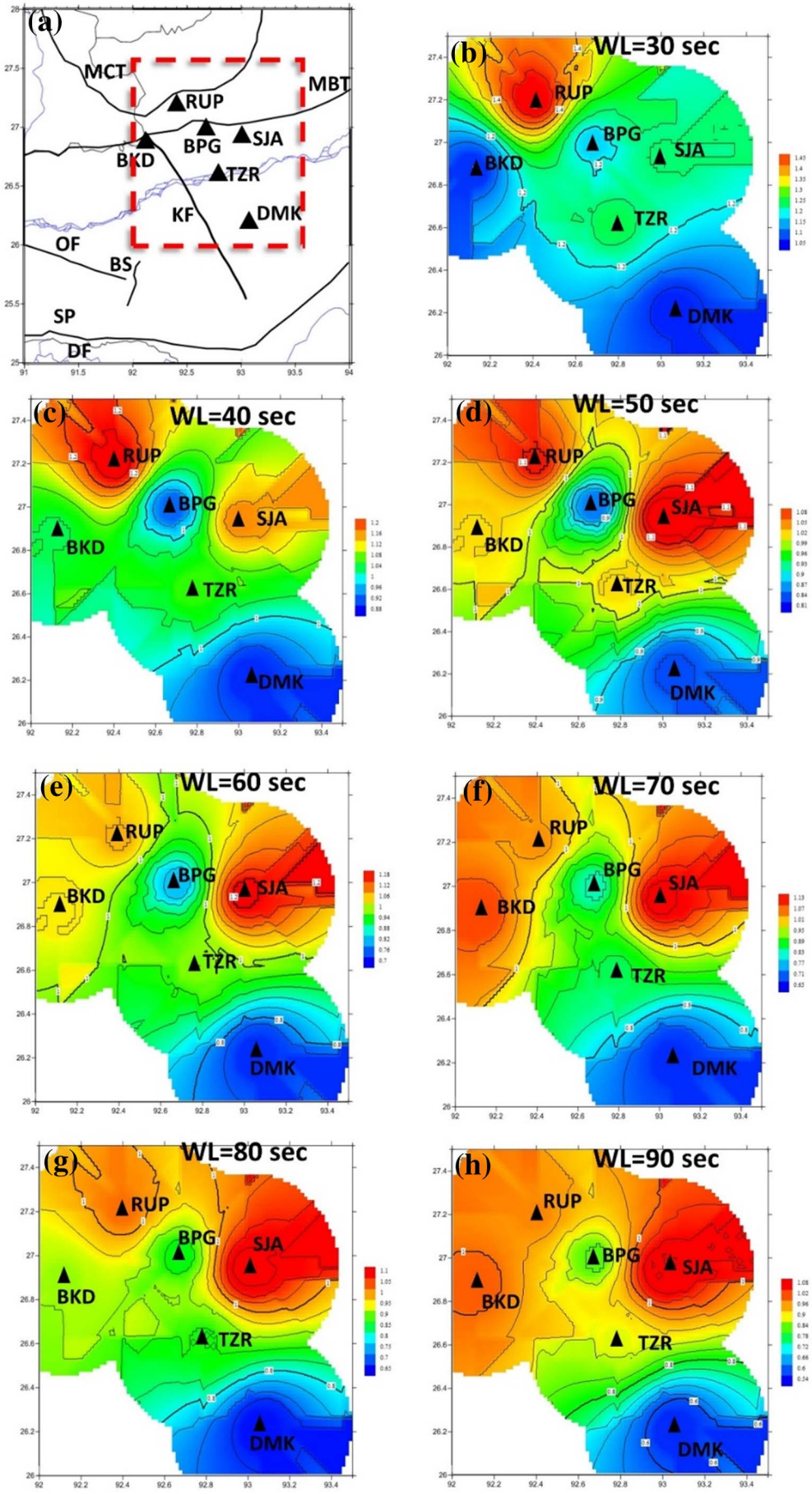

Fig. 8. (a) The study region and the dotted box represents the area selected for the contour plot. (b) to (h) Examples of the spatial distribution of frequency dependence (n) of coda Q. Triangles denote stations used to draw maps. The scale indicates the maximum and minimum values of n obtained for each coda window length.

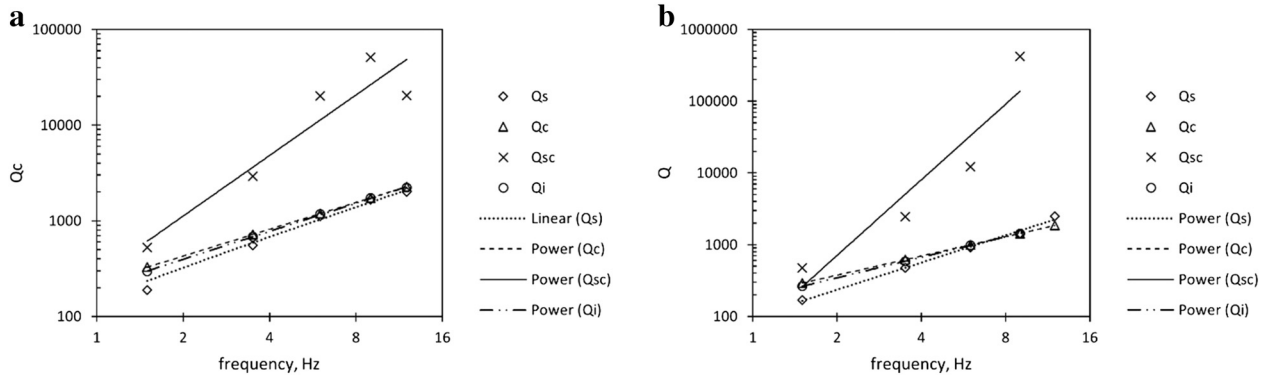

Fig. 9. Variation of Q_C, Q_S, Q_i and Q_{SC} with frequency for stations (a) TZR and (b) BKD.

window, it is observed that the values of Q_0 for station DMK was less than the other sites. But with increase in coda window length, it rises almost linearly which can be seen in Fig. 7 (c), (d), (e), (f), (g) and (h) [for Q_0].

In order to further investigate this, we have found a noticeable evidence from Bora et al. (2017), as they reported that as DMK is located on an alluvial plain. These alluvial plain tends to acts as "filters" to seismic waves by attenuating motions at certain frequencies and amplifying it at other frequency. But with increase in coda window length (for WL $>$ *30* s), the values of Q_0 increase which may be due to the higher penetration depth since the lithosphere becomes more homogeneous with depth.

The estimated "*n*" values for all the six stations indicate very strong frequency dependence of Q_C. For window length *30* and *40* s, the frequency dependence parameter at station RUP is almost high (Fig. 8 (b) and (c)) compared to the other stations. But as we move from window length *50* to *90* s (Fig. 8 (d) to Fig. 8 (h)), the "*n*" values of station RUP, BKD, SJA are high compared to the other remaining stations. Thus, higher frequency dependency determined for higher lapse times shows that these sites are more heterogeneous than the remaining sites. This is also supported by the variation of Q_0 with lapse time for these three stations. For instance, BKD receiver site is characterized by higher values of Q_0 within window length from *30* to *50* s (as seen from Table 3 and Fig. 7(b) to (d)). These higher values of Q_0 shows a noticeable difference from the other stations and it may reflect regional geological differences. For window length *60* to *90* s, the values of Q_0 (for station BKD, RUP and SJA) are lower than the remaining stations. These lower Q_0 values reflect strong scattering effects arising either due to the dense faulting or complex structure beneath these three stations. As it is well known that lesser the value of Q_0 implies higher seismic activity. The reason behind this may be attributed to the presence of MBT (main boundary thrust) near all these three stations, which makes them highly active as higher values of *n* indicate active region. It is worthy to mention here that MBT is one of the main tectonic features of Himalayas region and most earthquakes that occur in the Himalayas are along these tectonic features. It is claimed that the Kopili fault intersects the Himalaya and caused displacement and curvilinear structure at the MBT and MCT (Main Central Thrust) zone (Kayal et al., 2010, 2012). Since it is well known that the Kopili fault segmented the Shillong Platue into two parts namely, the Shillong Massif and the Mikir Massif. Consequently, a strong seismic activity down to *50 km* is recorded along this fault (Kayal et al., 2012). Regarding the seismic activity, it is already reported that the Kopili Fault had been the source zone of two past earthquake; the 1869 earthquake occurred towards southeast end of the Kopili fault and 1943 earthquake occurred at the centre of the fault zone. Bhattacharya et al. (2008) relocated the local networks events and identified the intense seismic activity along the Kopili fault that continues to the MCT in the Bhutan Himalaya.

It is interesting to see from Fig. 8 (d), (e), (f), (g) & (h) that for window length *50* to *90* s, the values of *n* for station SJA is almost constant ($\sim$*1.1*), which is a characteristic feature of vigorous scattering in a heterogeneous crust (Hazarika et al., 2009; Padhy and Subhadra, 2010).

Apart from these, Fig. 7 (d) and (e) imply some anomaly in values of Q_0. Similar anomaly is also observed in case of frequency parameter *n* as there is a certain fall in *n* values at window length *50* s. This may be due to the velocity anomaly at depth *210–220 km* as discussed in previous section. As from Table 5, it is clear that for *50* to *60* s window length the coda wave penetration is in between *220* $\pm$ *10 km*.

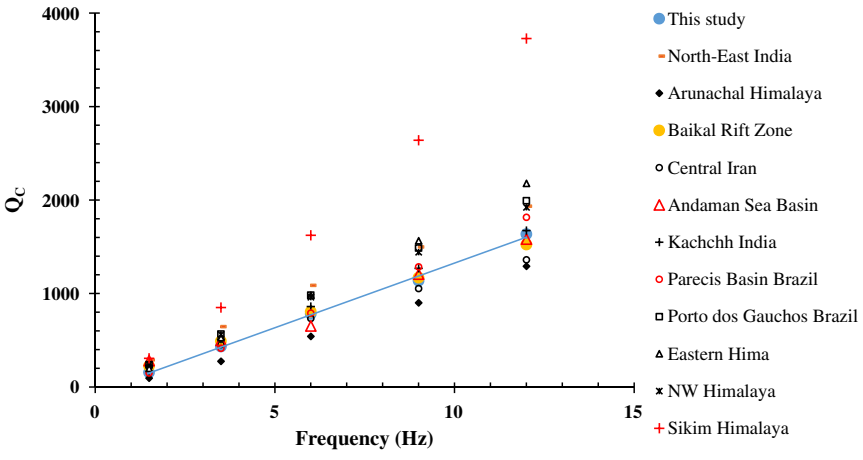

Fig. 10. Comparison of our estimated Q_C with Q_C from other parts of the world. For comparison only those values are selected which have used *40* s window.

Table 1
Location of six stations with hypocentral parameter.

Station name	Latitude (degrees)	Longitude (degrees)	Elevation (meter)	Ground type	Epicentral distance (km)		
					ED_{min}	ED_{max}	ED_{mean} ± sd
BKD	26.89	92.11	210	Hard rock	60	218	120 ± 50
BPG	26.99	92.67	130	Hard rock	11	251	97 ± 68
DMK	26.21	93.06	200	Alluvium	17	194	83 ± 54
RUPA	27.20	92.40	1470	Hard rock	38	195	88 ± 38
SJA	26.93	92.99	150	Hard rock	20	245	129 ± 71
TZR	26.61	92.78	140	Hard rock	54	200	103 ± 49

Table 2
Parameters of band-pass filter showing central frequencies with respective low and high cut off frequencies.

Band	Low cutoff frequency (Hz)	Central frequency (Hz)	High cutoff frequency (Hz)
1	1	1.5	2
2	2	3.5	5
3	4	6	8
4	6	9	12
5	9	12	15

6.5. Relation between Q_S and Q_C

Aki (1981) first discussed about the relation between attenuation of S wave and coda wave. After that, several authors including Frankel and Wennerberg (1987), Abdel-Fattah et al. (2008), Padhy et al. (2011), etc. have discussed the relationship between these two crucial factors. A comparison of Q_C and Q_S obtained by Bora and Biswas (2017) shows that in our study region the Q_S is more than Q_C for the entire frequency band. This implies increased scattering attenuation, which causes more seismic energy to be distributed into the coda from the direct pulse with increasing time, which can be referred as high-frequency coda enrichment. Frankel and Wennerberg (1987) advised that if scattering attenuation is important, it would cause S wave to decay faster than the coda waves, which is shown in our estimation.

6.6. Separation of intrinsic and scattering attenuation

To some extent, the concrete correlation between scattering and intrinsic attenuation is still under debate. In our study we have endeavored to resolve the two mechanisms with the help of the Wennerberg's (1993) method. In order to proceed, we have used the values of Q_S estimated by Bora and Biswas (2017), as they used the same dataset for Kopili region. Towards estimation of Q_S, they used coda-normalization method developed by Yoshimoto et al. (1993). From their estimated values of Q_S, it is observed that except for two station (TZR and BKD for *80* s window length) the values of Q_S is greater than Q_C. As opinioned by Zeng et al. (1991), Q_C should be greater than Q_S which is the basis of Wennerberg (1993) method.

According to this method, we can estimate intrinsic (Q_i) and scattering (Q_{SC}) attenuation by following relations,

$$\frac{1}{Q_S} = \frac{1}{Q_i} + \frac{1}{Q_{SC}} \tag{4}$$

Wennerberg (1993) showed that Q_C can be related to Q_i and Q_{SC} as

$$\frac{1}{Q_C} = \frac{1}{Q_i} + \frac{1 - 2\delta(\tau)}{Q_{SC}} \tag{5}$$

where, $1\text{-}2\delta(\tau) = -1/(4.44 + 0.738\tau)$ and $\tau = \omega t/Q_{SC}$, ω is the angular frequency, t is the lapse time and τ is the mean free time.

Assuming Q_S as the quality factor of the direct S wave, Qi and Q_{SC} can be expressed as

$$\frac{1}{Q_{SC}} = \frac{1}{2\delta(\tau)}\left(\frac{1}{Q_S} - \frac{1}{Q_C(\tau)}\right) \tag{6}$$

$$\frac{1}{Q_i} = \frac{1}{2\delta(\tau)}\left(\frac{1}{Q_C(\tau)} + \frac{2\delta(\tau) - 1}{Q_S}\right) \tag{7}$$

Combining the aforementioned equations, Q_{SC} can be derived from the positive root of the quadratic equation given as

$$(Q_C - Q_S)4.44Q_{SC}^2 + Q_{SC}[0.738\omega t(Q_C - Q_S) - 5.44Q_S Q_C] - 0.738\omega t Q_S Q_C = 0 \tag{8}$$

By taking $t = 90$ s and using the values of Q_C for *80* s window length, we have estimated the values of Q_i and Q_{SC} for two stations TZR and BKD. The estimated values are given in Table 6.

It is observed that in different sections of the world, the contribution of intrinsic and scattering effect in attenuation varies (e.g., Bianco et al., 1999, 2002; Mukhopadhyay et al., 2006). There was considerable confusion about whether coda attenuation is basically controlled by intrinsic or scattering attenuation (Aki and Chouet, 1975; Singh and Hermann, 1983; Frankel and Wennerberg, 1987; Fehler and Sato, 2003). As observed from the Fig. 9 and Table 6, the estimated values of Q_C and Q_i are almost similar, which suggest that the coda attenuation is basically dominant by intrinsic attenuation as compared to scattering attenuation, which is supported by the seismic albedo (B_0). In Kopili region, B_0 varies inversely with frequency (Table 6). As proposed by Wu (1985), B_0 varies from *0* to *1* and it describe the proportion of energy loss dominated by intrinsic attenuation ($B_0 < 0.5$) or scattering attenuation ($B_0 > 0.5$). The extinction length varies from *70* to *103 km* and *62* to *116 km* for BKD and TZR respectively. Noteworthy fact is that at lapse time window *80* s for two stations (TZR and BKD), the intrinsic attenuation increases with depth. Since, compaction of rock rises with increase in depth resulting in less relative motion of grain, as such, the increase in intrinsic attenuation can be assumed to be fueled by this phenomenon.

6.7. Coda Q and temperature

Among many other physical phenomena that affect Q, temperature also probably plays a dominant role below the upper crust (Sarker and Abers, 1999). It is widely accepted that the Q_C value in high temperature or magma intrusion area is usually low. Sarker and Abers (1999) have shown that the Q^{-1} variations are a reasonable proxy for temperature variations. Gao (1992) suggested that, if coda mainly reveals the intrinsic Q, it should be very sensitive to temperature and the content of liquid within the detected body. Conversely, if the activities are produced by small stress variations, consideration of coda Q may be less sensitive to the change in stress in comparison to temperature; it may thus be less sensitive to the stress related precursors. The data of geothermal structure for the crust and mantle indicate that the heat flow for the region is as high as *51–70 mW/m²* (data from International Heat Flow Commission). Priestley et al. (2008) reported that the distribution of earthquake depths throughout this region is consistent with a generic global view of seismicity in which earthquakes occur in (1)

Table 3
Average Vertical quality factor values at each frequency band obtained from local earthquakes in the Kopili Fault zone.

WL (sec)	Stations	1.5	3.5	6	9	12	$Q_C(f) = Q_o f^n$
30	BKD	188.79	341.22	808.59	1248.41	1590.03	$Q_C = 110f^{1.076}$
	RUP	113.53	409.45	790.94	3044.75	1829.69	$Q_C = 63f^{1.509}$
	BPG	96.343	281.58	600.18	671.11	1234.50	$Q_C = 62f^{1.176}$
	SJA	128.10	312.21	496.24	1156.23	1702.81	$Q_C = 70f^{1.238}$
	TZR	106.59	324.92	592.16	970.41	1496.77	$Q_C = 65f^{1.248}$
	DMK	88.179	624.05	604.99	772.85	1005.62	$Q_C = 84f^{1.072}$
	Whole area	114.16	374.28	666.22	1649.08	1563.22	$Q_C = 63f^{1.330}$
40	BKD	208.28	522.20	1208.61	1455.86	1641.76	$Q_C = 146f^{1.040}$
	RUP	147.05	453.57	865.36	1541.65	1927.74	$Q_C = 91f^{1.26}$
	BPG	139.61	382.17	664.15	760.12	978.569	$Q_C = 107f^{0.93}$
	SJA	154.02	383.62	638.98	1040.19	2005.69	$Q_C = 90f^{1.172}$
	TZR	148.14	426.43	684.50	896.82	1546.76	$Q_C = 101f^{1.066}$
	DMK	185.31	378.82	721.03	826.12	1228.13	$Q_C = 129f^{0.895}$
	Whole area	154.91	431.97	781.39	1136.16	1634.44	$Q_C = 102f^{1.119}$
50	BKD	226.09	511.35	1085.46	1301.47	1859.99	$Q_C = 151f^{1.015}$
	RUP	192.47	495.56	951.39	1408.40	1854.02	$Q_C = 125f^{1.10}$
	BPG	174.33	534.17	774.33	871.28	1102.21	$Q_C = 145f^{0.86}$
	SJA	184.56	461.80	740.01	1271.20	2155.99	$Q_C = 110f^{1.139}$
	TZR	182.84	521.89	744.81	970.03	1831.22	$Q_C = 126f^{1.018}$
	DMK	249.67	438.46	681.48	922.87	1564.42	$Q_C = 164f^{0.837}$
	Whole area	193.78	502.35	831.72	1134.52	1790.25	$Q_C = 131f^{1.030}$
60	BKD	232.11	570.02	1144.91	1540.25	1977.98	$Q_C = 155f^{1.047}$
	RUP	205.77	528.70	1026.05	1334.78	1978.53	$Q_C = 137f^{1.075}$
	BPG	213.01	588.19	919.16	974.15	1267.03	$Q_C = 175f^{0.83}$
	SJA	190.94	583.92	1138.21	1766.29	2263.26	$Q_C = 124f^{1.202}$
	TZR	213.90	631.94	817.76	1098.39	2108.08	$Q_C = 150f^{0.998}$
	DMK	289.10	489.32	716.92	955.98	1374.93	$Q_C = 205f^{0.726}$
	Whole area	216.77	576.21	930.05	1183.15	1917.73	$Q_C = 151f^{0.998}$
70	BKD	243.53	650.64	1398.43	1728.93	2373.76	$Q_C = 163f^{1.101}$
	RUP	231.11	583.95	1077.84	1648.07	1925.82	$Q_C = 156f^{1.047}$
	BPG	246.54	581.38	1081.91	1112.63	1434.36	$Q_C = 192f^{0.844}$
	SJA	214.97	630.31	1242.65	1899.73	2358.82	$Q_C = 140f^{1.172}$
	TZR	253.22	690.28	838.26	1051.67	1869.21	$Q_C = 191f^{0.865}$
	DMK	338.57	627.89	894.86	1031.28	1504.83	$Q_C = 260f^{0.679}$
	Whole area	248.97	637.02	1002.98	1335.16	1821.00	$Q_C = 180f^{0.936}$
80	BKD	249.50	772.30	1175.62	1832.47	1505.07	$Q_C = 202f^{0.93}$
	RUP	248.39	550.90	903.91	1635.52	2018.86	$Q_C = 158f^{1.026}$
	BPG	260.47	623.12	1054.04	1360.02	1709.94	$Q_C = 195f^{0.87}$
	SJA	245.50	686.13	1157.85	2232.29	2428.27	$Q_C = 159f^{1.139}$
	TZR	282.18	724.68	906.70	1145.48	2230.68	$Q_C = 203f^{0.89}$
	DMK	395.28	666.56	899.87	1087.36	1755.34	$Q_C = 291f^{0.66}$
	Whole area	274.42	659.43	947.44	1416.22	2050.02	$Q_C = 191f^{0.934}$
90	BKD	261.74	689.43	1661.09	2170.67	1689.70	$Q_C = 196f^{1.012}$
	RUP	262.13	542.94	948.92	1501.47	1932.80	$Q_C = 170f^{0.98}$
	BPG	266.26	1093.42	1024.25	1430.55	1813.84	$Q_C = 240f^{0.846}$
	SJA	254.98	669.14	1277.12	2103.05	2417.69	$Q_C = 166f^{1.118}$
	TZR	331.31	781.64	991.34	1436.24	2502.55	$Q_C = 230f^{0.895}$
	DMK	435.90	721.18	959.50	1226.69	1435.22	$Q_C = 348f^{0.57}$
	Whole area	304.62	701.52	1044.03	1523.37	2135.39	$Q_C = 213f^{0.913}$

'wet' upper crustal material to a temperature of $\sim 350\ ^\circ C$, or (2) higher temperatures in dry granulite-facies lower crust or (3) mantle that is colder than $\sim 600\ ^\circ C$. The physical mechanism that Q_o usually exhibits low values in the tectonically active regions still needs more in-depth analysis. Mitchell (1995) pointed out that tectonic activity generates heat and the heat initiates hydrothermal reactions in the upper mantle and, perhaps, in the crust. The fluids, caused by the hydrothermal reactions after release, flow upward through cracks and permeable rocks. Sometimes, they predominantly habitat in the upper crust. As such, regions of low Q can be, in general, characterized by high temperatures and heat flow. Further, the cracks filled with liquids, as aforementioned enhances the scattering, resulting in loss of the energy of the waves. This might be the reason of low Q in the tectonically active regions. The data of geothermal structure for the crust and mantle indicate that the heat flow for the region is as high as $51–70\ mW/m^2$ (data from International Heat Flow Commission). Thus the low coda Q_o value obtained in the present study is supported by the heat flow and high temperature.

6.8. Comparison with global data

We have compared values of different areas with our results. The worldwide attenuation studies have shown that Q_o is normally high in stable regions and low in active tectonic regions. Based on that it was reported that $Q_o < 200$ and $n > 0.7$, for tectonically active areas such as Japan (Aki and Chouet, 1975), Washington (Havskov et al., 1989), Charlevoix region-Canada (Woodgold, 1994), Parkfield, California (Hellweg et al., 1995), Koyna-India (Mandal and Rastogi, 1998), southeastern Sicily (Italy) (Giampiccolo et al., 2004), southwestern Iran (Rahimi and Hamzehloo, 2008), Taiwan (Chung et al., 2009), Andaman Sea basin (Padhy et al., 2011), Georgia (Shengelia et al., 2011), Turkey (Sertçelik, 2012), Italy (de Lorenzo et al., 2013), eastern Iran (Mahood, 2014). On the other hand, for, $Q_o > 600$ and $n < 0.4$, have been acquired for tectonically inactive areas such as, United States (Singh and Hermann, 1983), Canadian Shield (Hasegawa, 1985), Iberian Peninsula-Spain (Pujades, 1990), southeastern Canada (Atkinson and Mereu, 1992), Eastern North America (Atkinson and Boore, 1995), southeastern Canada and the northeastern United States (Atkinson,

Table 4
The variations of the attenuation parameters (Q_0, n) with the lapse time window.

WL	Station	Q_0	$\pm \Delta Q_0$	n	$\pm \Delta n$
30	BKD	110	8	1.08	0.09
	RUP	63	12	1.51	0.25
	BPG	62	5	1.18	0.09
	SJA	70	6	1.24	0.11
	TZR	65	1	1.25	0.26
	DMK	84	18	1.07	0.28
40	BKD	146	12	1.04	0.11
	RUP	91	3	1.26	0.04
	BPG	107	7	0.93	0.09
	SJA	90	8	1.17	0.09
	TZR	101	6	1.07	0.07
	DMK	129	6	0.9	0.06
50	BKD	151	7	1.02	0.06
	RUP	125	2	1.1	0.03
	BPG	145	14	0.86	0.12
	SJA	110	6	1.14	0.07
	TZR	126	10	1.02	0.1
	DMK	164	11	0.84	0.09
60	BKD	155	6	1.04	0.05
	RUP	137	5	1.08	0.04
	BPG	175	15	0.83	0.1
	SJA	124	4	1.2	0.04
	TZR	150	14	0.99	0.12
	DMK	205	8	0.73	0.05
70	BKD	163	9	1.1	0.07
	RUP	156	5	1.05	0.04
	BPG	192	14	0.84	0.09
	SJA	140	5	1.17	0.05
	TZR	191	17	0.87	0.11
	DMK	260	10	0.68	0.05
80	BKD	202	23	0.92	0.15
	RUP	158	6	1.03	0.05
	BPG	195	11	0.87	0.07
	SJA	159	8	1.14	0.07
	TZR	203	19	0.88	0.12
	DMK	291	17	0.66	0.08
90	BKD	196	28	1.01	0.18
	RUP	170	4	0.98	0.03
	BPG	240	35	0.84	0.18
	SJA	166	6	1.12	0.05
	TZR	230	17	0.89	0.09
	DMK	348	2	0.57	0.01

Table 5
Average estimated values of the ellipsoid axes (a, b) and depth with the lapse time window and corresponding attenuation co-efficient.

WL (sec)	a (km)	b (km)	Depth (km)	γ (Km^{-1})	$\pm \Delta\gamma$ (Km^{-1})
30	190	183	207	0.0080	0.002253
40	199	192	216	0.0073	0.000726
50	208	201	225	0.0065	0.000415
60	216	210	234	0.0060	0.000493
70	225	219	243	0.0055	0.000404
80	234	228	252	0.0052	0.000387
90	243	237	261	0.0049	0.000362

2004).

For comparison, it is desirable to have almost similar lapse time window, since the values of Q_C rises with increasing lapse time window length. That's why, only those studies are selected for comparison which have used a coda window length of 40s. Fig. 10 shows the comparison of few global as well as regional studies. Referring to Fig. 10, there are equivalent trends for regions with similar tectonic activities and the Kopili region clearly follows the trend for regions with high seismic activities. Results of the regionalization for coda Q suggest that the entire area is highly heterogeneous in nature.

Table 6
Values of Q_S, Q_C (for window length of 80 s), Q_i, Q_S and Seismic albedo (B_0) corresponding to different central frequencies for TZR and BKD station.

Station	Central frequency	Q_S	Q_C	Q_{SC}	Q_i	B_0
BKD	1.5	189	328	525	295	0.359881
	3.5	556	721	2921	686	0.190322
	6	1111	1191	20,163	1175	0.055099
	9	1667	1736	51,233	1723	0.032537
	12	2000	2269	20,471	2216	0.097699
TZR	1.5	169	291	473	262	0.357256
	3.5	476	619	2469	589	0.192715
	6	909	1000	12,138	982	0.074883
	9	1428	1434	418,004	1432	0.003416
	12	2500	1853			

7. Conclusions

In this work, coda-Q (Q_C) has been estimated for the Kopili fault zone using a single back-scattering model of S-coda envelopes. Based on our analysis following inferences are made.

1. The average Q_C values, estimated for Kopili region, and their frequency-dependent relationships show that the medium is highly heterogeneous.
2. The frequency-dependent relationships for Kopili region are estimated as $(63 \pm 6)f^{(1.33 \pm 0.11)}$ for 30 s window and $(213 \pm 5)f^{(0.91 \pm 0.03)}$ for 90 s window length.
3. The attained Coda-Q reflects an average attenuation property for a surface area of about *181,468* km^2 to a depth of about *261 km* covered by the coda waves generated by the earthquakes considered in this study.
4. We have found an increase in the quality factor and decrease in the frequency parameter and attenuation coefficient with lapse time window (and accordingly depth) which may implicate that the crust and upper part of the earth's mantle are more heterogeneous compared to its lowest layers. Variations of attenuation parameters with depth are connected with the velocity discontinuity of the region at depth *210–220 km* as there arises sharp changes in attenuation coefficient and frequency parameter which are supported by the available velocity anomaly and temperature variation of previously reported data.
5. There is a striking difference that exists between attenuation properties of DMK and the other stations. While the frequency dependence parameter is high for stations RUP, BKD and SJA, as compared to the other remaining three stations. This is primarily due to the presence of main boundary thrust near these stations.
6. The whole study area is dominated by mainly scattering attenuation but, we can see an increase in intrinsic attenuation with depth in TZR and BKD receiver sites.
7. The comparison of estimated Q_0 for these regions of north east India indicates that the attenuation in Kopili fault zone follows the trends of zones with higher seismic activity.

Although the present study is based on a limited data set, still the estimated relationships $Q_C(f) = Q_0 f^n$ give considerable information about seismic wave attenuation characteristics of this study region of NER India. The estimation of Q_C in Kopili region will be an important parameter for the prediction of large earthquakes, assessment of seismic hazard, and for better understanding of tectonics, the seismicity, and the engineering seismology (Jin and Aki, 1988). This work will act as a basic building block when the entire NER, India will be intended to cover as part of future work.

Acknowledgements

We are grateful to the two anonymous reviewers for their

constructive criticisms and valuable comments which enable us to improve the manuscript. We express our gratitude to the editor for his helpful suggestions. We thank Ministry of Earth Sciences, Government of India for supporting this work through grant [MoES/P.O.(Seismo)/1(214)/2014]. Author NB acknowledges MoES for financial support.

References

Abdel-Fattah, A.K., Morsy, M., El-Hady, S., Kim, K.Y., Sami, M., 2008. Intrinsic and scattering attenuation in the crust of the Abu Dabbab area in the Eastern Desert of Egypt. Phys. Earth Planet. Inter. 168 (1–2), 103–112.

Aki, K., 1969. Analysis of the Seismic Coda of Local Earthquakes as Scattered Waves. 74(2). pp. 615–631.

Aki, K., 1980. Attenuation of shear-waves in the lithosphere for frequencies from 0.05 to 25 Hz. Phys. Earth Planet. Inter. 21 (1), 50–60.

Aki, K., 1981. Source and Scattering Effects on the Spectra of Small Local Earthquakes. 71(6). pp. 1687–1700.

Aki, K., Chouet, B., 1975. Origin of coda waves: source, attenuation, and scattering effects. J. Geophys. Res. 80 (23), 3322.

Atkinson, G.M., 2004. Empirical attenuation of ground-motion spectral amplitudes in Southeastern Canada and the Northeastern United States. Bull. Seismol. Soc. Am. 94 (3), 1079–1095.

Atkinson, G.M., Boore, D.M., 1995. Ground-motion relations for Eastern North America. Bull. Seismol. Soc. Am. 85 (1), 17–30.

Atkinson, G.M., Mereu, R.F., 1992. The shape of ground motion attenuation curves in Southeastern Canada. Bull. Seismol. Soc. Am. 82 (5), 2014–2031.

Bhattacharya, P.M., Mukhopadhyay, S., Majumdar, R.K., Kayal, J.R., 2008. 3-D seismic structure of the Northeast India region and its implications for local and regional tectonics. J. Asian Earth Sci. 33 (1–2), 25–41.

Bianco, F., Castellano, M., Del Pezzo, E., Ibanez, J.M., 1999. Attenuation of short-period seismic waves at Mt Vesuvius, Italy. Geophys. J. Int. 138 (1), 67–76.

Bianco, F., Del Pezzo, E., Castellano, M., Ibanez, J., Di Luccio, F., 2002. Separation of intrinsic and scattering seismic attenuation in the southern Apennine zone, Italy. Geophys. J. Int. 150 (1), 10–22.

Biswas, R., Baruah, S., Bora, D.K., Kalita, A., Baruah, S., 2013a. The effects of attenuation and site on the spectra of microearthquakes in the Shillong region of Northeast India. Pure Appl. Geophys. 170 (11), 1833–1848. http://dx.doi.org/10.1007/s00024-012-0631-0.

Biswas, R., Baruah, S., Bora, D., 2013b. Influnce of attenuation and site on micro-earthquakes' spectra in Shillong Region of Northeast India: a case study. Acta Geophysica 61, 886–904.

Bora, N., Biswas, R., 2017. Quantifying regional body wave attenuation in a seismic prone zone of Northeast India. Pure Appl. Geophys. 174 (5), 1953–1963.

Bora, N., Biswas, R., Bora, D., 2017. Assessing attenuation characteristics prevailing in a seismic prone area of NER India. J. Geophys. Eng. 14, 1368–1381. http://dx.doi.org/10.1088/1742-2140/aa7d11.

Carcolé, E., Sato, H., 2010. Spatial distribution of scattering loss and intrinsic absorption of short-period S waves in the lithosphere of Japan on the basis of the multiple lapse time window analysis of Hi-net data. Geophys. J. Int. 180, 268–290.

Chung, T.W., Lees, J.M., Yoshimoto, K., Fujita, E., Ukawa, M., 2009. Intrinsic and scattering attenuation of the Mt Fuji region, Japan. Geophys. J. Int. 177 (3), 1366–1382.

Dasović, I., Herak, M., Herak, D., 2013. Coda-Q and its lapse time dependence analysis in the interaction zone of the Dinarides, the Alps and the Pannonian Basin. Phys. Chem. Earth 63, 47–54.

Del Pezzo, E., Allotta, R., Patane, D., 1990. Dependence of Qc (coda Q) on coda duration time interval: model or depth effect? Bull. Seismol. Soc. Am. 80 (4), 1028–1033.

Dobrynina, A., 2013. Seismic Waves Attenuation in the Lithosphere of the Northern Basin and Range Province. 15(12). pp. 31038.

Dobrynina, A.A., Sankov, V.A., Chechelnitsky, V.V., Déverchère, J., 2016. Spatial changes of seismic attenuation and multiscale geological heterogeneity in the Baikal Rift and surroundings from analysis of coda waves. Tectonophysics 675, 50–68.

Dojo, M., Hiramatsu, Y., 2017. Spatial variation in coda Q in the northeastern part of Niigata-Kobe Tectonic Zone, central Japan: implication of the cause of a high strain rate zone. Earth Planets Space 69, 76. http://dx.doi.org/10.1186/s40623-017-0663-x.

Fehler, M., Sato, H., 2003. Coda. Pure Appl. Geophys. 160, 541–554.

Frankel, A., Wennerberg, L., 1987. Energy-flux model of seismic coda: separation of scattering and intrinsic attenuation. Bull. Seismol. Soc. Am. 77 (4), 1223–1251.

Frankel, A., 2015. Decay of S-wave amplitudes with distance for earthquakes in the Charlevoix, Quebec, area: Effects of radiation pattern and directivity. Bull. Seismol. Soc. Am. 105, 850–857.

Gao, L.-S., 1992. Physical Meaning of the Coda Envelopes. Springer, Berlin, Heidelberg, pp. 391–403.

Giampiccolo, E., Gresta, S., Rasconà, F., 2004. Intrinsic and scattering attenuation from observed seismic codas in southeastern Sicily (Italy). Phys. Earth Planet. Inter. 145 (1), 55–66.

Guo, M.Q., Fu, L.Y., Ba, J., 2009. Comparison of stress-associated coda attenuation and intrinsic attenuation from ultrasonic measurements. Geophys. J. Int. 178 (1), 447–456.

Gupta, H.K., Singh, S.C., Dutta, T.K., Saikia, M.M., 1984. Recent investigations of North East India seismicity. In: Gongu, G., Xing-Yuan, M. (Eds.), Proceedings of the International Symposium on Continental Seismicity and Earthquake Prediction. Seismological Press, Beijing, pp. 63–71.

Gupta, S.C., Singh, V.N., Kumar, A., 1995. Attenuation of Coda Waves in the Garhwal Himalaya, India. Phys. Earth Planet. Inter. 87 (3–4), 247–253.

Gupta, S.C., Teotia, S.S., Rai, S.S., Gautam, N., 1998. Coda Q estimates in the Koyna region, India. In: Q of the Earth: Global, Regional, and Laboratory Studies. Basel, Birkhäuser Basel, pp. 713–731.

Hanks, T.C., McGuire, R.K., 1981. The character of high frequency strong ground motion. Bull. Seismol. Soc. Am. 71, 2071–2095.

Hasegawa, H.S., 1985. Attenuation of Lg waves in the Canadian shield. Bull. Seismol. Soc. Am. 75 (6), 1569–1582.

Havskov, J., Ottemoller, L., 2005. SEISAN (Version 8.1): The Earthquake Analysis Software for Windows, Solaris, Linux, and Mac OSX Version 8.0. pp. 254.

Havskov, J., Malone, S., Mcclurg, D., Crosson, R., 1989. Coda-Q for the state of Washington. Bull. Seismol. Soc. Am. 79 (4), 1024–1038.

Hazarika, D., Baruah, S., Gogoi, N.K., 2009. Attenuation of coda waves in the Northeastern region of India. J. Seismol. 13 (1), 141–160.

Hazarika, P., Ravi Kumar, M., Kumar, D., 2013. Attenuation character of seismic waves in Sikkim Himalaya. Geophys. J. Int. 195 (1), 544–557.

Hellweg, M., Spudich, P., Fletcher, J.B., Baker, L.M., 1995. Stability of coda *Q* in the region of Parkfield, California: view from the U.S. Geological Survey Parkfield Dense Seismograph Array. J. Geophys. Res. Solid Earth 100 (B2), 2089–2102.

Hiramatsu, Y., Sawada, A., Yamauchi, Y., Ueyama, S., Nishigami, K., Kurashimo, E., the Japanese University Group of the Joint Seismic Observations at NKTZ, 2013. Spatial variation in coda Q and stressing rate around the Atotsugawa fault zone in a high strain rate zone, central Japan. Earth Planets Space 65, 115–119. http://dx.doi.org/10.5047/eps.2012.08.012.

Irandoust, M.A., Sobouti, F., Rahimi, H., 2016. Lateral and depth variations of coda Q in the Zagros region of Iran. J. Seismol. 20 (1), 197–211.

Jin, A., Aki, K., 1988. Spatial and temporal correlation between coda Q and seismicity in China. Bull. Seismol. Soc. Am. 78 (2), 741–769.

Jin, A., Aki, K., 2005. High-resolution maps of Coda Q in Japan and their interpretation by the brittle-ductile interaction hypothesis. Earth Planets Space 57, 403–409. http://dx.doi.org/10.1186/BF03351825.

Kayal, J.R., Arefiev, S.S., Barua, S., Hazarika, D., Gogoi, N., Kumar, A., Chowdhury, S.N., Kalita, S., 2006. Shillong plateau earthquakes in Northeast India region: complex tectonic model. Curr. Sci. 91 (1), 109–114.

Kayal, J.R., Arefiev, S.S., Baruah, S., Tatevossian, R., Gogoi, N., Sanoujam, M., Gautam, J.L., Hazarika, D., Borah, D., 2010. The 2009 Bhutan and Assam felt earthquakes (Mw 6.3 and 5.1) at the Kopili fault in the northeast Himalaya region. Geomat. Nat. Haz. Risk 1 (3), 273–281.

Kayal, J.R., Arefiev, S.S., Baruah, S., Hazarika, D., Gogoi, N., Gautam, J.L., Baruah, S., Dorbath, C., Tatevossian, R., 2012. Large and great earthquakes in the Shillong plateau-Assam valley area of Northeast India Region: pop-up and transverse tectonics. Tectonophysics 532–535, 186–192.

Knopoff, L., Hudson, J.A., 1964. Scattering of elastic waves by small inhomogeneities. J. Acoust. Soc. Am. 36, 338–343.

Kumar, N., Parvez, I.A., Virk, H.S., 2005. Estimation of coda wave attenuation for NW Himalayan region using local earthquakes. Phys. Earth Planet. Inter. 151 (3–4), 243–258.

Kumar, R., Gupta, S.C., Singh, S.P., Kumar, A., 2016a. The attenuation of high-frequency seismic waves in the lower Siang region of Arunachal Himalaya: Qα, Qβ, Qc, Qi, and Qs. Bull. Seismol. Soc. Am. 106 (4), 1407–1422.

Kumar, D., Reddy, D.V., Pandey, A.K., 2016b. Paleoseismic investigations in the Kopili fault zone of north East India: evidences from liquefaction chronology. Tectonophysics 674, 65–75.

Kundu, B., Gahalaut, V.K., 2013. Tectonic geodesy revealing geodynamic complexity of the Indo-Burmese Arc Region, North East India. Curr. Sci. 104 (7), 920–933.

de Lorenzo, S., Del Pezzo, E., Bianco, F., 2013. Qc, Qβ, Qi and Qs attenuation parameters in the Umbria–Marche (Italy) region. Phys. Earth Planet. Inter. 218, 19–30.

Mahood, M., 2014. Attenuation of high-frequency seismic waves in Eastern Iran. Pure Appl. Geophys. 171 (9), 2225–2240.

Mandal, P., Rastogi, B.K., 1998. A frequency-dependent relation of coda Q c for Koyna-Warna region, India. Pure Appl. Geophys. 153 (1), 163–177. Retrieved May 2, 2017. https://doi.org/10.1007/s000240050190.

Mitchell, B.J., 1995. Anelastic structure and evolution of the continental crust and upper mantle from seismic surface wave attenuation. Rev. Geophys. 33 (4), 441.

Mukhopadhyay, S., Sharma, J., 2010. Attenuation characteristics of Garwhal-Kumaun Himalayas from analysis of coda of local earthquakes. J. Seismol. 14 (4), 693–713.

Mukhopadhyay, S., Tyagi, C., Rai, S.S., R., W. & M.P., S, 2006. The attenuation mechanism of seismic waves in Northwestern Himalayas. Geophys. J. Int. 167 (1), 354–360.

Negi, S.S., Paul, A., Joshi, A., Kamal, 2014. Body wave crustal attenuation in the Garhwal Himalaya, India. In: Pure Appl. Geophysics. Springer Basel.

Novelo-Casanova, D.A., Martínez-Bringas, A., Valdés-González, C., 2006. Temporal variations of Qc-1 and B-values associated to the December 2000–January 2001 volcanic activity at the Popocatepetl volcano, Mexico. J. Volcanol. Geotherm. Res. 152 (3–4), 347–358.

Oldham, R.D., 1899. Report on the great earthquake of 12th June 1897. Mem. Geol. Surv. India 29, 1–379.

Padhy, S., Subhadra, N., 2010. Attenuation of high-frequency seismic waves in Northeast India. Geophys. J. Int. 181 (1), 453–467.

Padhy, S., Subhadra, N., Kayal, J.R., 2011. Frequency-dependent attenuation of body and coda waves in the Andaman Sea basin. Bull. Seismol. Soc. Am. 101 (1), 109–125.

Parvez, I.A., Sutar, A.K., Mridula, M., Mishra, S.K., Rai, S.S., 2008. Coda Q Estimates in the Andaman Islands Using Local Earthquakes. Pure Appl. Geophys. 165, 1861–1878. http://dx.doi.org/10.1007/s00024-008-0399-4.

Poddar, M.C., 1950. The Assam earthquake of 15th August 1950. Indian Miner. 4,

167–176.
Priestley, K., James, J., Mckenzie, D., 2008. Lithospheric structure and deep earthquakes beneath India, the Himalaya and Southern Tibet. Geophys. J. Int. 172 (1), 345–362.
Pujades, L., 1990. Seismic attenuation in Iberia using the coda-Q method. Geophys. J. Int. 103, 135–145.
Pulli, J., 1984. Attenuation of coda waves in New England. Bull. Seismol. Soc. Am. 74 (4), 1149–1166.
Rahimi, H., Hamzehloo, H., 2008. Lapse time and frequency-dependent attenuation of coda waves in the Zagros continental collision zone in Southwestern Iran. J. Geophys. Eng. 5 (2), 173–185.
Ramesh, D.S., Kumar, M.R., Devi, E.U., Raju, P.S., Yuan, X., 2005. Moho geometry and upper mantle images of Northeast India. Geophys. Res. Lett. 32 (14), 1–4.
Rautian, T., Khalturin, V., 1978. The use of the coda for determination of the earthquake source Spectrum. Bull. Seismol. Soc. Am. 68 (4), 923–948.
Sarker, G., Abers, G.A., 1999. Lithospheric temperature estimates from seismic attenuation across range fronts in Southern and Central Eurasia. Geology 27 (5), 427–430.
Sato, H., 1977. Energy propagation including scattering effects single isotropic scattering approximation. J. Phys. Earth 25 (1), 27–41.
Sato, H., 1987. A precursor like change in coda excitation before the western Nagano earthquake (Ms = 6.8) of 1984 in central Japan. J. Geophys. Res. 92, 1356–1360.
Sato, H., Fehler, M., 1998. Scattering and Attenuation of Seismic Waves in Heterogeneous Earth. AIP Press, Springer Verlag, New York, New York.
Scherbaum, F., Kisslinger, C., 1985. Coda Q in the Adak seismic zone. Bull. Seismol. Soc. Am. 75 (2), 615–620.
Sedaghati, F., Pezeshk, S., 2016. Estimation of the coda-wave attenuation and geometrical spreading in the New Madrid seismic zone. Bull. Seismol. Soc. Am. 106 (4), 1482–1498.
Sertçelik, F., 2012. Estimation of coda wave attenuation in the East Anatolia fault zone, Turkey. Pure Appl. Geophys. 169 (7), 1189–1204.
Sharma, B., Teotia, S.S., Kumar, D., Raju, P.S., 2009. Attenuation of P- and S-waves in the Chamoli region, Himalaya, India. Pure Appl. Geophys. 166 (12), 1949–1966.
Shengelia, I., Javakhishvili, Z., Jorjiashvili, N., 2011. Coda wave attenuation for three regions of Georgia (Sakartvelo) using local earthquakes. Bull. Seismol. Soc. Am. 101 (5), 2220–2230.
Singh, S.K., Hermann, R.B., 1983. Regionalization of crustal Q in the continental United States. J. Geophys. Res. 88, 527–538.
Singh, C., Basha, S.K., Shekar, M., Chadha, R.K., 2012. Spatial variation of coda wave attenuation in the Southern Indian shield and its implications. Geol. Acta 10 (3), 309–318.
Singh, A.P., Purnachandra Rao, N., Ravi Kumar, M., Hsieh, M.-C., Zhao, L., 2017. Role of the Kopili fault in deformation tectonics of the Indo-Burmese arc inferred from the rupture process of the 3 January 2016 M W 6.7 Imphal earthquake. Bull. Seismol. Soc. Am. 107 (2), 1–7.
Spudich, P., Bostwick, T., 1987. Studies of the seismic coda using an earthquake cluster as a deeply buried seismograph array. J. Geophys. Res. 92 (B10), 526–546.
Steck, L.K., Prothero, W.A., Scheimer, J., 1989. Site-dependent Coda Q at Mono Craters, California. 79(5). pp. 1559–1574.
Stewart, R., 1984. And the Rise and Fall of a Seismic Pulse R. Stewart. pp. 793–805.
Tripathi, J.N., Singh, P., Sharma, M.L., 2012. Variation of seismic coda wave attenuation in the Garhwal region, Northwestern Himalaya. Pure Appl. Geophys. 169 (1–2), 71–88.
Wei, W., Zhao, D., Xu, J., Zhou, B., Shi, Y., 2016. Depth variations of P-wave azimuthal anisotropy beneath mainland China. Sci. Rep. 6 (August), 29614.
Wennerberg, L., 1993. Multiple-scattering interpretations of coda-Q measurements. Bull. Seismol. Soc. Am. 83 (1), 279–290.
Woodgold, C.R.D., 1994. Coda Q in the Charlevoix, Quebec, region: lapse-time dependence and spatial and temporal comparisons. Bull. Seismol. Soc. Am. 84 (4), 1123–1131.
Wu, R.-S., 1985. Multiple Scattering and Energy Transfer of Seismic Waves-Separation of Scattering Effect from Intrinsic Attenuation — I. Theoretical Modelling. pp. 57–80.
Yoshimoto, K., Sato, H., Ohtake, M., 1993. Frequency dependent attenuation of P and S waves in the Kanto area, Japan, based on the coda-normalization method. Geophys. J. Int. 114 (1), 165–174.
Zelt, B.C., Dotzev, N.T., Ellis, R.M., Rogers, G.C., 1999. Coda Q in Southwestern British Columbia, Canada. Bull. Seismol. Soc. Am. 89 (4).
Zeng, Y., Su, F., Aki, K., 1991. Scattered wave energy propagation in a random isotropic scattering medium: I. Theory, J. Geophys. Res. 96, 607–619.